Optimal Third-Harmonic Current Injection for Asymmetrical Multiphase Permanent Magnet Synchronous Machines

Andrea Cervone, *Student Member, IEEE*, Marko Slunjski, *Student Member, IEEE*, Emil Levi, *Fellow, IEEE*, and Gianluca Brando

***Abstract*—This article proposes a modeling approach and an optimization strategy to exploit a third-harmonic current injection for the torque enhancement in multiphase isotropic permanent magnet synchronous machines with nonsinusoidal back electromotive forces. The modeling approach is based on a proper vector space decomposition and on the associated rotational transformation, aimed to properly select a set of stator current space vectors to be controlled. It is presented for a generic (i.e., asymmetrical, with an arbitrary angular shift) winding configuration. The injection strategy is related to the choice of a constant synchronous current set aimed at minimizing the average stator winding losses for a given reference torque by using the first and the third spatial harmonics of the air-gap flux density. The optimal solution has been found analytically and has been developed in detail for a selected set of asymmetrical winding configurations. Both the numerical and experimental results are in good agreement with the theoretical analysis.**

***Index Terms*—Asymmetrical machines, multiphase drives, nonsinusoidal back electromotive force (EMF), power loss minimization, surface mounted permanent magnet synchronous machine (PMSM), third-harmonic current injection.**

I. Introduction

Multiphase electrical machines represent viable alternative to traditional three-phase ones in many high-power and high-reliability applications, ranging from wind energy generation to electrical traction (e.g., electric/hybrid vehicles, more electric aircraft, ship propulsion, etc.) [1]–[3]. Among the many benefits they offer, multiphase machines can continue to operate at reduced power even after multiple phase faults, as long as the healthy phases are able to produce a rotating air-gap flux-density field [1]–[3]. Moreover, for a given rated power and voltage, a multiphase machine's rated current is lower than in its three-phase counterpart, allowing to employ converters with reduced current ratings, thus leading to more reliable operation and higher efficiency [1]. Finally, the higher number of phases leads to additional degrees of freedom, which can be exploited for additional control purposes [1]–[7]. This includes independent utilization of different spatial harmonics of the air-gap flux density generated by the stator currents to enhance torque production [1]–[7].

For permanent magnet synchronous machines (PMSMs), this property can be exploited to increase the torque/current ratio by properly coupling the stator's and rotor's contribution for different viable spatial harmonics [4]–[7]. This approach leads to a set of nonsinusoidal currents in steady-state conditions and, consequently, corresponds to a higher order current harmonic injection. In particular, when only the third-order spatial harmonic is exploited, a proper third-harmonic injection strategy can be implemented [4]–[7]. In this case, the optimization problem is reduced to the identification of the optimal ratio between the two stator-driven harmonic contributions to the air-gap flux density.

In the case of machines characterized by an odd number of phases and a symmetrical winding configuration, it has been verified that, based on the stator winding loss minimization criterion, the optimal injection ratio coincides with the one between the corresponding magnets' induced back electromotive forces (EMFs) [4]–[13]. Several applications of these strategies can be found, especially for five-phase machines [9]–[17].

On the contrary, the higher order harmonic injection for asymmetrical winding configurations has been rarely discussed in the literature, the exceptions being [18]–[22]. While [18] considers the fifth and the seventh harmonic injection, in [19] and [20], [21] a third-harmonic injection has been investigated for a six-phase induction machine and a six-phase PMSM, respectively. However, the torque enhancement requires connection of the winding's neutral point to either an additional inverter leg or to the midpoint of the capacitor bank in the dc link, to allow the free circulation of the injected harmonic. The third-harmonic amplitude is equal in all phases.

As an alternative, in [22] the authors have shown how the torque enhancement can be applied in an asymmetrical nine-phase PMSM with a single but isolated neutral point. In this

Manuscript received November 12, 2019; revised January 27, 2020 and March 3, 2020; accepted March 8, 2020. Date of publication March 25, 2020; date of current version December 8, 2020. *(Corresponding author: Andrea Cervone.)*

Andrea Cervone and Gianluca Brando are with the Department of Electrical Engineering and Information Technology, University of Naples Federico II, 80125 Naples, Italy (e-mail: andrea.cervone@unina.it; gianluca.brando@unina.it).

Marko Slunjski and Emil Levi are with the Faculty of Engineering and Technology, Liverpool John Moores University, L3 3AF Liverpool, U.K. (e-mail: m.slunjski@2017.ljmu.ac.uk; e.levi@ljmu.ac.uk).

Color versions of one or more of the figures in this article are available online at http://ieeexplore.ieee.org.

Digital Object Identifier 10.1109/TIE.2020.2982099

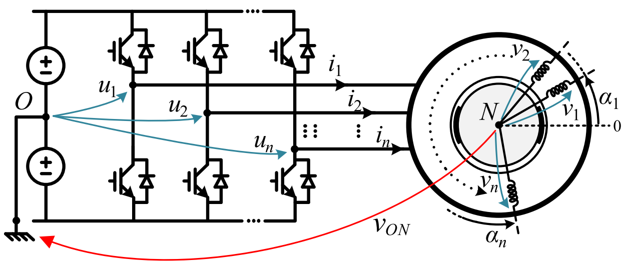

Fig. 1. System architecture for an n-phase PMSM with a single neutral point.

case, the optimal injection ratio is modified with respect to the symmetrical configuration. This article extends the results given in [22] by formulating the optimization problem with respect to a generic n-phase PMSM. The approach, by exploiting a proper vector space decomposition (VSD) and the associated rotational transformation, is able to highlight how each current component contributes to the electromagnetic torque and to the average power losses (see Section II). Consequently, the generalized optimization problem can be formulated in a compact way; the solution can be found analytically and it only depends on the magnitude of the magnets' induced fluxes (responsible for the electromagnetic torque) and on the winding configuration (responsible for the power losses) (see Section III).

The proposed strategy has been particularized for selected examples of machines with an asymmetrical winding configuration (see Section IV). Both numerical and an experimental validation has also been performed employing a nine-phase asymmetrical machine (see Section V). Section VI concludes this article.

II. Mathematical Model

The machine under analysis is assumed to have n identical stator windings arranged in P_p pole pairs and distributed along the machine's stator periphery so that their magnetic axes have an electrical phase displacement of α_k (with $k = 1, \ldots, n$) with respect to an arbitrary reference. The windings are assumed to be connected into a single neutral point and supplied by a voltage source inverter; the architecture is schematically represented in Fig. 1.

The magnetic flux density in the air-gap generated by the rotor's permanent magnets (PMs), once decomposed in a Fourier series with respect to the stator electric angle, is in general given by the superposition of an infinite number of spatial harmonics. These harmonics produce in each kth stator winding a flux which can be expressed as

$$\lambda_k(\theta) = \sum_h \lambda_{Mh} \cos\left(h(\theta - \alpha_k) + \varphi_h\right) \tag{1}$$

where λ_{Mh} and φ_h are the magnitude and the phase displacement of the flux contribution due to the hth flux density spatial harmonic, while θ denotes the electric angle between the rotor reference axis and the stator reference one.

A. Per-Phase Electrical Equations

Assuming linearity, the mathematical model of a magnetically isotropic PMSM with a single isolated neutral point (see Fig. 1) is represented by the set of equations [1]

$$\begin{cases} [u_{\mathrm{ph}}] + v_{\mathrm{ON}} \cdot [1_{n\times 1}] = [v_{\mathrm{ph}}] \\ \quad = [R] \cdot [i_{\mathrm{ph}}] + [L] \cdot \frac{\mathrm{d}}{\mathrm{d}t}[i_{\mathrm{ph}}] + [e_{\mathrm{ph}}] \\ [1_{n\times 1}]^{\mathrm{T}} \cdot [i_{\mathrm{ph}}] = \sum_{k=1}^{n} i_k = 0 \end{cases} \tag{2}$$

where $[u_{\mathrm{ph}}]$, $[e_{\mathrm{ph}}]$, and $[i_{\mathrm{ph}}]$ are the sets of the inverter's leg voltages, PM induced back-EMFs, and stator winding currents, v_{ON} is the voltage between the inverter's dc link midpoint O and the machine's neutral point N, $[v_{\mathrm{ph}}]$ is the set of the stator winding voltages, $[R]$ is the winding resistances matrix ($[R] = R \cdot [I_{n\times n}]$), $[L]$ is the stator winding inductance matrix (which includes both the mutual and the leakage contributions), and $[1_{n\times 1}] = [1, 1, \ldots, 1]^{\mathrm{T}}$ is the unitary $n \times 1$ column vector.

The PM induced back-EMFs are expressed as

$$e_k = \frac{\mathrm{d}\lambda_k}{\mathrm{d}t} = \omega \cdot \frac{\partial \lambda_k}{\partial \theta} = -\omega \cdot \sum_h h \cdot \lambda_{Mh} \sin\left(h(\theta - \alpha_k) + \varphi_h\right) \tag{3}$$

where $\omega = \mathrm{d}\theta/\mathrm{d}t$ is the machine's rotor electrical speed.

B. Torque Expression in the Space Vector Formalism

By applying a set of currents to the machine's stator windings, the magnetic flux density in the air-gap is modified. This new current-dependent field can be once again decomposed in an infinite number of spatial harmonics, each of which can be identified through an hth order space vector

$$\mathbf{i}_h = i_{xh} + \mathrm{j} \cdot i_{yh} = \sqrt{2/n} \cdot \sum_{k=1}^{n} i_k \cdot \mathrm{e}^{\mathrm{j}h\alpha_k}. \tag{4}$$

By expressing each space vector $\mathbf{i}_h$ in a hth spatial harmonic synchronous reference frame through the complex rotation

$$\mathbf{i}_h^{\langle dq \rangle} = i_{dh} + \mathrm{j} \cdot i_{qh} = \mathbf{i}_h \cdot \mathrm{e}^{-\mathrm{j}(h\theta + \varphi_h)} \tag{5}$$

and by considering (1), the electromagnetic torque developed by the PMSM can be analytically expressed as

$$\begin{aligned} T_{em} &= P_p \cdot \sum_{k=1}^{n} i_k \cdot (\partial \lambda_k / \partial \theta) \\ &= P_p \cdot \sum_h h \cdot \lambda_{Mh} \cdot \left[\sum_{k=1}^{n} i_k \cdot \sin\left(h(\theta - \alpha_k) + \varphi_h\right) \right] \\ &= P_p \cdot \sum_h h \cdot \lambda_{Mh} \cdot \left[\sqrt{n/2} \cdot \mathrm{Im}\{\mathbf{i}_h \cdot \mathrm{e}^{-\mathrm{j}(h\theta + \varphi_h)}\} \right] \\ &= \sum_h \left(P_p \cdot \sqrt{n/2} \cdot h \cdot \lambda_{Mh} \right) \cdot i_{qh} = \sum_h \kappa_h \cdot i_{qh} \end{aligned} \tag{6}$$

where $\kappa_h = P_p \cdot \sqrt{n/2} \cdot h \cdot \lambda_{Mh}$ is a constant gain related to the hth harmonic. Only the quadrature components of the space vectors, by interacting with the corresponding harmonics of the PM induced fluxes, are responsible for the torque production. However, it is important to observe that, since the phase currents form an n-dimensional set, only up to n scalar components of the space vectors can be set arbitrarily.

Moreover, the winding configuration further reduces the number of controllable components by forcing to zero the sum of all the phase currents [second equation in (2)]: this condition can be conveniently expressed in terms of a zero-sequence component constraint as $i_0 = (\sum_{k=1}^{n} i_k)/\sqrt{n} = 0$.

C. Choice of the VSD Transformation

As for standard multiphase machines, the mathematical model can be reformulated through a variable transformation known as Vector Space Decomposition [1]–[3]. The transformed current set $[i_{\mathrm{VSD}}]$ should be chosen in order to include a set of space vector components $\{i_{\mathrm{x}h}, i_{\mathrm{y}h}\}$ to be controlled and the zero-sequence component i_0 (constrained to zero by hardware configuration). The correlation between the transformed current set $[i_{\mathrm{VSD}}]$ and the phase current set $[i_{\mathrm{ph}}]$ is

$$[i_{\mathrm{VSD}}] = [C] \cdot [i_{\mathrm{ph}}] \quad \Leftrightarrow \quad [i_{\mathrm{ph}}] = [T] \cdot [i_{\mathrm{VSD}}] \tag{7}$$

with $[C]$ the generalized Clarke's transformation matrix.

As per (4), the components of each hth space vector $\mathbf{i}_h$ can be introduced into $[i_{\mathrm{VSD}}]$ through the set of rows

$$[C_h] = \sqrt{\frac{2}{n}} \cdot \begin{bmatrix} \cos(h\,\alpha_1) & \cos(h\,\alpha_2) & \cdots & \cos(h\,\alpha_n) \\ \sin(h\,\alpha_1) & \sin(h\,\alpha_2) & \cdots & \sin(h\,\alpha_n) \end{bmatrix} \tag{8}$$

while i_0 can be introduced through the row $[C_0] = [1_{n\times 1}]^{\mathrm{T}}/\sqrt{n}$.

Obviously, $[C]$ needs to be a full rank matrix to guarantee the existence of its inverse $[T] = [C]^{-1}$ and, therefore, preserve the number of state variables. As a result, a chosen set of space vectors can be controlled only if the corresponding rows in the transformation matrix are linearly independent from each other.

For an odd number of phases it is possible to control at most $(n - 1)/2$ space vectors at the same time, while, for an even number of phases, the number of independently controllable space vectors is $(n - 2)/2$—in this case, to get a full-rank transformation matrix, after introducing the corresponding $(n - 2)$ rows as per (8) and the zero sequence row $[C_0]$, $[C]$ can be completed by introducing a second zero-sequence component i_{0^-} through an additional row $[C_{0^-}]$.

To establish whether a set of space vectors can be freely controlled, it is sufficient to compute the rank of the matrix built by considering the corresponding rows $[C_h]$ [defined as per (8)] and the zero-sequence row $[C_0]$—indeed, when some rows are linearly dependent on some others, there are certain algebraic constraints between the corresponding space vector components. Therefore, to get full control of both $\mathbf{i}_1$ and $\mathbf{i}_3$, which will be exploited in Section III by the proposed strategy, the Clarke transformation matrix should be built as

$$[C] = \begin{bmatrix} [C_1] \\ [C_3] \\ \vdots \\ ([C_{0^-}]) \\ [C_0] \end{bmatrix} \text{ with } [i_{\mathrm{VSD}}] = [i_{\mathrm{x}1}, i_{\mathrm{y}1}, i_{\mathrm{x}3}, i_{\mathrm{y}3}, \ldots, (i_{0^-}), i_0]^{\mathrm{T}}. \tag{9}$$

In (9), the higher order rows should be chosen, wherever possible, to take advantage of the space vectors associated with the highest torque gain factors κ_h (usually the ones which drive the lowest odd-order spatial harmonics). Once the set $[i_{\mathrm{VSD}}]$ has been chosen, its relationship with any other hth space vector components $\{i_{\mathrm{x}h}, i_{\mathrm{y}h}\}$ is found to be

$$[i_{\mathrm{x}h}\ i_{\mathrm{y}h}]^{\mathrm{T}} = [C_h] \cdot [i_{\mathrm{ph}}] = [C_h] \cdot [T] \cdot [i_{\mathrm{VSD}}]. \tag{10}$$

In the case of a symmetrical machine with an odd number of phases the magnetic axes are $\alpha_k = (k - 1)\cdot(2\pi/n)$ and it can be verified that, by choosing the space vectors linked to the smallest $(n - 1)/2$ odd-order spatial harmonics, the resulting Clarke matrix $[C]$ is guaranteed to be unitary (i.e., invertible and such that $[T] = [C]^{-1} = [C]^{\mathrm{T}}$). This property is, however, not guaranteed in a generic configuration, as exemplified for the asymmetrical nine-phase PMSM in [22].

D. Choice of the Rotational Transformation

Once the Clarke's transformation matrix $[C]$ has been built to control a given set of space vectors, the VSD current set $[i_{\mathrm{VSD}}]$ can be linked to the corresponding synchronous set $[i_{dq}]$ through a rotational transformation

$$[i_{\mathrm{dq}}] = [\mathrm{D}](\theta) \cdot [i_{\mathrm{VSD}}] \quad \Leftrightarrow \quad [i_{\mathrm{VSD}}] = [\mathrm{D}]^{-1}(\theta) \cdot [i_{\mathrm{dq}}] \tag{11}$$

Given (5), the rotational matrix $[D](\theta)$ can be obtained by properly combining a set of submatrices $[D_h](\theta)$ built as

$$\begin{aligned} \begin{bmatrix} i_{\mathrm{d}h} \\ i_{\mathrm{q}h} \end{bmatrix} &= [D_h](\theta) \cdot \begin{bmatrix} i_{\mathrm{x}h} \\ i_{\mathrm{y}h} \end{bmatrix} \\ &= \begin{bmatrix} \cos(h\theta + \varphi_h) & \sin(h\theta + \varphi_h) \\ -\sin(h\theta + \varphi_h) & \cos(h\theta + \varphi_h) \end{bmatrix} \cdot \begin{bmatrix} i_{\mathrm{x}h} \\ i_{\mathrm{y}h} \end{bmatrix}. \end{aligned} \tag{12}$$

The rotational matrix associated to (9), which selects the $\mathbf{i}_1^{<dq>}$ and $\mathbf{i}_3^{<dq>}$ components, takes the block-diagonal form

$$[D](\theta) = \begin{bmatrix} [D_1](\theta) & [0_{2\times 2}] & \cdots & ([0_{2\times 1}]) & [0_{2\times 1}] \\ [0_{2\times 2}] & [D_3](\theta) & \cdots & ([0_{2\times 1}]) & [0_{2\times 1}] \\ \vdots & \vdots & \ddots & \vdots & \vdots \\ ([0_{1\times 2}]) & ([0_{1\times 2}]) & \cdots & (1) & (0) \\ [0_{1\times 2}] & [0_{1\times 2}] & \cdots & (0) & 1 \end{bmatrix} \tag{13}$$

with $[i_{dq}] = [i_{\mathrm{d}1}, i_{\mathrm{q}1}, i_{\mathrm{d}3}, i_{\mathrm{q}3}, \ldots, (i_{0^-}), i_0]^{\mathrm{T}}$. Generally speaking, once the set $[i_{\mathrm{VSD}}]$ contains both the real and imaginary part of each chosen space vector $\mathbf{i}_h$, the rotational matrix, built by combining the submatrices defined as per (12), can be verified to be unitary (i.e., $[D]^{-1}(\theta) = [D]^{\mathrm{T}}(\theta)$).

E. Power Loss Expression

Considering (7) and (11) and neglecting all losses except for those in the stator windings, the instantaneous power losses can be expressed in terms of the transformed current set $[i_{dq}]$

$$p = R \cdot \sum_{k=1}^{n} i_k^2 = R \cdot [i_{\mathrm{ph}}]^{\mathrm{T}} \cdot [i_{\mathrm{ph}}] = R \cdot [i_{dq}]^{\mathrm{T}} \cdot [G](\theta) \cdot [i_{dq}] \tag{14}$$

with $[G](\theta) = [D](\theta)\cdot[T]^{\mathrm{T}}\cdot[T]\cdot[D]^{\mathrm{T}}(\theta)$. Then, the average power losses can be found by averaging p along a full rotor cycle. For a constant synchronous current set $[i_{dq}]$ each component is independent of θ and the result is expressed as

$$P = (1/2\pi) \cdot \int_0^{2\pi} p(\theta)\mathrm{d}\theta = R \cdot [i_{dq}]^{\mathrm{T}} \cdot [H] \cdot [i_{dq}] \tag{15}$$

where $[H] = (1/2\pi) \cdot \int_0^{2\pi} [G](\theta)\mathrm{d}\theta$.

It can be verified that all the nondiagonal terms of $[G](\theta)$ are trigonometric functions with a zero average value over a full cycle of θ and that the diagonal terms corresponding to the same hth space vector have an equal average value $H_h > 0$ over a full electric rotation angle. Therefore, the matrix $[H]$ related to (9) and (13) is positive definite and assumes the diagonal for

$$[H] = \begin{bmatrix} H_1 & 0 & 0 & 0 & \cdots & (0) & 0 \\ 0 & H_1 & 0 & 0 & \cdots & (0) & 0 \\ 0 & 0 & H_3 & 0 & \cdots & (0) & 0 \\ 0 & 0 & 0 & H_3 & \cdots & (0) & 0 \\ \vdots & \vdots & \vdots & \vdots & \ddots & \vdots & \vdots \\ (0) & (0) & (0) & (0) & \cdots & (H_{0^-}) & (0) \\ 0 & 0 & 0 & 0 & \cdots & (0) & H_0 \end{bmatrix}. \tag{16}$$

To summarize, once $[C]$ has been chosen, both $[T]$ and $[D](\theta)$ are univocally identified. Consequently, it is possible to compute the instantaneous loss weighting matrix $[G](\theta)$, from which, by operating an element-by-element average process, the matrix $[H]$ is derived. For a symmetrical machine, since $[C]$ is unitary, it follows that $[G](\theta) = [H] = [I_{n\times n}]$.

F. Transformed Electrical Equations

Once the transformation matrices $[C]$ and $[D](\theta)$ have been chosen, they can be applied to all the variables in (2). By using the VSD transformation (7) the model is modified as

$$\begin{cases} [u_{\mathrm{VSD}}] + v_{\mathrm{ON}} \cdot [c] = [v_{\mathrm{VSD}}] \\ \quad = R \cdot [i_{\mathrm{VSD}}] + [L_{\mathrm{VSD}}] \cdot \frac{\mathrm{d}}{\mathrm{d}t}[i_{\mathrm{VSD}}] + [e_{\mathrm{VSD}}] \\ i_0 = [0\ 0\ \cdots\ 0\ (0)\ 1] \cdot [i_{\mathrm{VSD}}] = 0 \end{cases} \tag{17}$$

with $[c] = [C]\cdot[1_{n\times 1}]$ and $[L_{\mathrm{VSD}}] = [C]\cdot[L]\cdot[T]$.

For a machine with a symmetrical winding configuration and an odd number of phases, the inductance matrix $[L]$ has a circular structure (i.e., $L_{j,k} = L_{j+1,k+1}$). If, again, the space vectors linked to the smallest $(n - 1)/2$ odd-order spatial harmonics are selected, the rows of the matrix $[C]$ (and, given the unitary property, also the columns of $[T] = [C]^{\mathrm{T}}$) are the eigenvectors of the matrix $[L]$. As a result, the matrix $[L_{\mathrm{VSD}}] = [C]\cdot[L]\cdot[C]^{\mathrm{T}}$ is diagonal and effectively performs the decoupling of the different components of the $[i_{\mathrm{VSD}}]$ set. On the contrary, for a generic configuration this property is not guaranteed (as shown in [22] for a nine-phase asymmetrical machine).

By applying the rotational transformation (11) to the system (17), the model becomes

$$\begin{cases} [u_{dq}] + v_{\mathrm{ON}} \cdot [g](\theta) = [v_{dq}] = R \cdot [i_{dq}] + \cdots \\ \quad \cdots + [L_{dq1}](\theta) \cdot \frac{\mathrm{d}}{\mathrm{d}t}[i_{dq}] + \omega \cdot [L_{dq2}](\theta) \cdot [i_{dq}] + [e_{dq}] \\ i_0 = [0\ \ 0\ \ \cdots\ \ 0\ \ (0)\ \ 1] \cdot [i_{dq}] = 0 \end{cases} \tag{18}$$

with $[g](\theta) = [D](\theta)\cdot[c]$, $[L_{dq1}](\theta) = [D](\theta)\cdot[L_{\mathrm{VSD}}]\cdot[D]^{\mathrm{T}}(\theta)$ and $[L_{dq2}](\theta) = [D](\theta)\cdot[L_{\mathrm{VSD}}]\cdot(\partial[D]^{\mathrm{T}}(\theta)/\partial\theta)$. Again, the different components of $[i_{dq}]$ can exhibit a coupling effect both through the transformed inductance matrices $[L_{dq1}](\theta)$, $[L_{dq2}](\theta)$ and through the term $v_{\mathrm{ON}} \cdot [g](\theta)$. Indeed, the neutral point potential shift v_{ON} generally depends not only on the voltage sets $[e_{dq}]$ and $[u_{dq}]$, but also on the current set $[i_{dq}]$—the formal relationship can be found by imposing the constraint $i_0 = 0$ and the subsequent condition $\mathrm{d}i_0/\mathrm{d}t = 0$ in the zero-sequence subspace equation of (18). Once substituted back in the other subspace equations, it allows to explicitly highlight the additional mutual coupling between the current components.

III. Optimal Third-Harmonic Injection Strategy

Standard field oriented control (FOC) algorithms, developed for isotropic PMSMs, only control the $i_{\mathrm{q}1}$ current component of the $[i_{dq}]$ set, while keeping all the other terms to zero. Consequently, the reference current $i_{q1}^* = T_{em}^*/\kappa_1$ is proportional to the desired torque T_{em}^* and the overall average power losses are $P_{\mathrm{FUND}} = R\ H_1\ (T_{em}^*/\kappa_1)^2$. For a constant rotor speed, the resulting reference phase currents are sinusoidal.

However, in the presence of significant higher order spatial harmonics in the PMs' induced flux density, it is possible to exploit the quadrature component of some higher order current space vectors as available degrees of freedom for the torque development. Then, given the higher number of degrees of freedom, it is possible to formulate an optimal strategy to choose the current references while keeping the supplied torque to the desired reference T_{em}^*.

The proposed strategy aims to minimize the average stator power losses for a given torque by using a constant synchronous current set $[i_{dq}^*]$. Under the reasonable hypothesis that all the even-order spatial harmonics are absent and that the odd-order ones with index $h \geq n$ are negligible, the torque expression (6) is a linear combination of the synchronous current set component contributions, which can be synthetically formulated by introducing the $n \times 1$ torque gain vector as

$$[\kappa] = P_p\sqrt{n/2} \cdot [0\ \lambda_{M1}\ 0\ 3\lambda_{M3}\ \cdots\ (0)\ 0]^{\mathrm{T}} \tag{19}$$

resulting in $T_{em} = [\kappa]^{\mathrm{T}} \cdot [i_{dq}]$. Since $[\kappa]$ is independent from θ, it allows for an optimization with a constant $[i_{dq}^*]$ vector.

Then, the simplest enhancement can be obtained through the control of the $i_{\mathrm{q}3}$ current component. In steady-state conditions at a constant speed, due to the 3θ rotation in the $[D](\theta)$ matrix, the application of a constant $i_{\mathrm{q}3}$ corresponds to a third-harmonic current injection into each phase current. All the other components of $[i_{dq}]$ can be set to zero not to interfere either with the torque development or with the power dissipation.

Then, the function to minimize is $P = R \cdot (H_1 i_{q1}^2 + H_3 i_{q3}^2)$, under the equality constraint represented by the reference torque development $T_{em}^* = \kappa_1 i_{q1} + \kappa_3 i_{q3}$.

The average power losses can be expressed as a function of the third-harmonic injection ratio $k = i_{\mathrm{q}3}/\, i_{\mathrm{q}1}$ as

$$P(k) = R \cdot (T_{em}^*)^2 \cdot (H_1 + H_3 k^2)/(\kappa_1 + \kappa_3 k)^2. \tag{20}$$

The function (20) is convex with respect to k and its minimum value can be found by forcing to zero its derivative $\partial P/\partial k$. The optimal injection ratio is

$$k_{\text{opt}} = (\kappa_3/\kappa_1)/(H_3/H_1) \tag{21}$$

and the corresponding optimal currents are

$$i_{q1}^* = \frac{H_3\kappa_1}{H_1\kappa_3^2 + H_3\kappa_1^2}T_{em}^*; \quad i_{q3}^* = \frac{H_1\kappa_3}{H_1\kappa_3^2 + H_3\kappa_1^2}T_{em}^*. \tag{22}$$

The average power losses with the optimal injection ratio are

$$P_{\text{opt}} = R\cdot(T_{em}^*)^2\cdot(H_1H_3)/(\kappa_3^2H_1 + \kappa_1^2H_3) \tag{23}$$

and can be compared to the ones generated by a traditional strategy which only exploits i_{q1}, leading to a ratio of

$$\eta_{\text{opt}} = P_{\text{opt}}/P_{\text{FUND}} = (\kappa_1^2H_3)/(\kappa_3^2H_1 + \kappa_1^2H_3). \tag{24}$$

From the set $[i_{dq}^*]$, whose i_{q1}^* and i_{q3}^* components are chosen via (22), the optimal phase current set $[i_{\text{ph}}^*]$ can be found by applying the inverse transformations (7) and (11).

IV. Application Examples

To highlight the generality of the approach, the strategy is discussed further on in detail for a selected set of phase numbers, for machines with asymmetrical winding topology.

A. Six-Phase Asymmetrical Machine

The machine windings can be grouped in two symmetrical three-phase sets $\{a_1, b_1, c_1\}$ and $\{a_2, b_2, c_2\}$ whose magnetic axes are mutually shifted by 30° electrically. The corresponding electrical angle set is $[\alpha] = [0°\ 120°\ 240°\,|\,30°\ 150°\ 270°]$. By examining via (8) the rows $[C_3]$ related to the third-harmonic space vector $\mathbf{i}_3$ one gets

$$[C_3] = \sqrt{1/3}\cdot\begin{bmatrix}1 & 1 & 1 & 0 & 0 & 0\\ 0 & 0 & 0 & 1 & 1 & 1\end{bmatrix}. \tag{25}$$

This set of rows is linearly dependent on the zero-sequence row $[C_0] = [1\ 1\ 1\ 1\ 1\ 1]/\sqrt{6}$. Since i_0 is constrained to zero by the single isolated neutral point configuration, i_{x3} and i_{y3} cannot be independently controlled at the same time. As a result, it is impossible to generate a rotating space vector $\mathbf{i}_3$ and the third-harmonic current injection cannot be exploited for the torque development unless there is an additional conductor allowing $i_0 \neq 0$ (as in [19]–[21] with the seventh inverter leg or with a direct connection of the neutral point N to the dc link midpoint O).

B. Nine-Phase Asymmetrical Machine

This configuration has been examined by the authors in [22]. The machine windings can be grouped in three symmetrical three-phase sets $\{a_1, b_1, c_1\}$, $\{a_2, b_2, c_2\}$, and $\{a_3, b_3, c_3\}$ whose magnetic axes are mutually shifted by 20° electrically; the corresponding electrical angle set is $[\alpha] = [0°\ 120°\ 240°\,|\,20°\ 140°\ 260°\,|\,40°\ 160°\ 280°]$.

It can be verified that the Clarke's matrix $[C]$ chosen to control the space vectors $\mathbf{i}_1$, $\mathbf{i}_3$, $\mathbf{i}_5$, and $\mathbf{i}_7$ is a full rank matrix. The evaluation of the $[H]$ matrix has been performed analytically, resulting in $H_1 = 1; H_3 = 5; H_5 = 1; H_7 = 1$; and $H_0 = 9$.

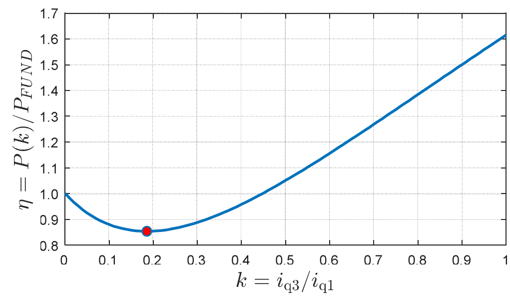

Fig. 2. Average losses in the asymmetrical nine-phase machine.

TABLE I
PM Induced Flux Harmonic Parameters

Harmonic Order h	1	3	5	7
λ_{Mh} [mWb]	385	119	38	7
φ_h [deg]	0°	≅ 180°	≅ 0°	≅ 165°

The strategy has been particularized with respect to the real prototype described in [22] and [23], whose PM flux parameters are summarized in Table I; for simplicity, the contribution of the harmonics with order $h > 7$ has been neglected.

Fig. 2 shows the normalized power losses obtained when both i_{q1} and i_{q3} are exploited for the torque development. Consistently with (21) and (24), the minimum power ratio $\eta \cong 0.85$ (highlighted by the red dot in Fig. 2) is obtained for $k \cong 0.19$ and corresponds to a 15% power loss reduction.

The optimal phase current waveforms and their spectra are depicted in Fig. 3, normalized by $I_{\text{FUND}} = (2/9)\cdot T_{em}^*/\lambda_{M1}$, which represents the peak phase current needed to supply the same torque by only exploiting the fundamental harmonic i_{q1}. In accordance with the analytical results, only the first and third-harmonics are present in the Fourier decomposition. The waveforms of each three-phase $\{a, b, c\}$ set are identical and just mutually shifted by 120°. Nevertheless, it can be immediately noticed that the different sets behave differently from each other. This results in the unequal injection of the third-harmonic components which, in order to satisfy the condition $i_0 = 0$, are not evenly distributed among the different phase sets. In particular, the magnitude in the first and the third set is equal, while the magnitude in the second set is $\sqrt{3}$ times higher. This unequal distribution of the currents leads to an unequal distribution of the power losses (31.3% for the first and third sets, 37.4% for the second set). Finally, it can also be noted that, despite the reduction of the root mean square (rms) with respect to the sole exploitation of i_{q1}, the normalized peak current values are higher than 1, and the $\{a_2, b_2, c_2\}$ is the most affected set.

C. Twelve-Phase Asymmetrical Machine

In this case, the machine windings can be grouped in four symmetrical three-phase sets $\{a_p, b_p, c_p\}$ (with $p = 1, \ldots, 4$), whose magnetic axes are mutually shifted by 15°. The machine parameters are still assumed to be the same as those in Table I.

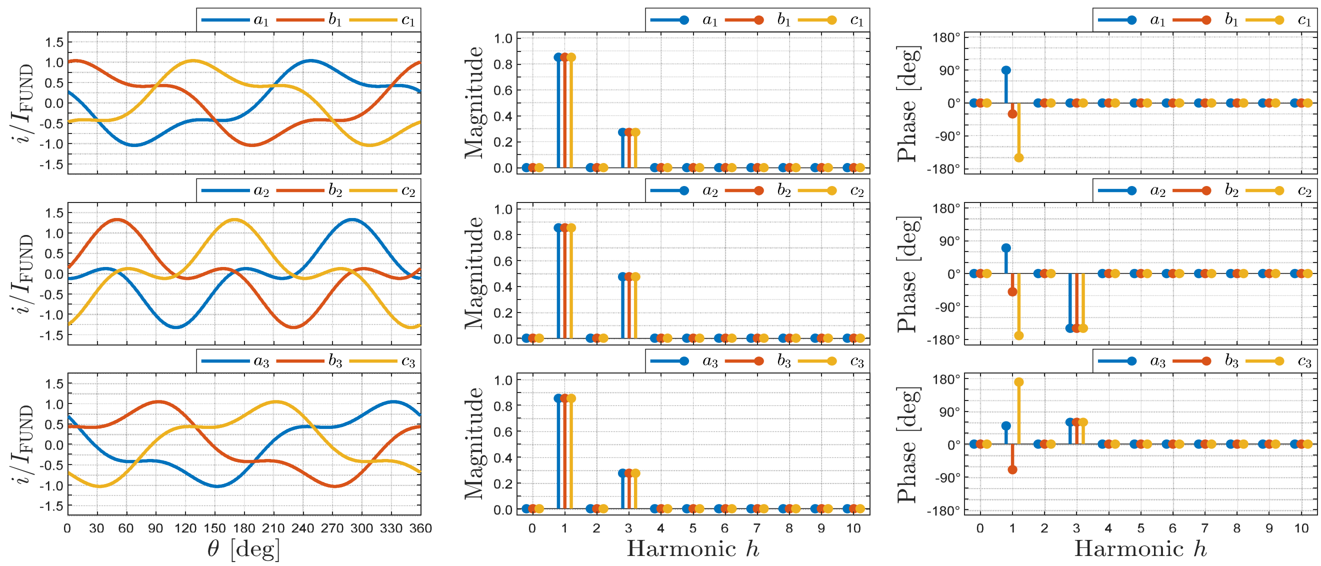

Fig. 3. Optimal phase current waveforms and harmonic spectra for the asymmetrical nine-phase machine.

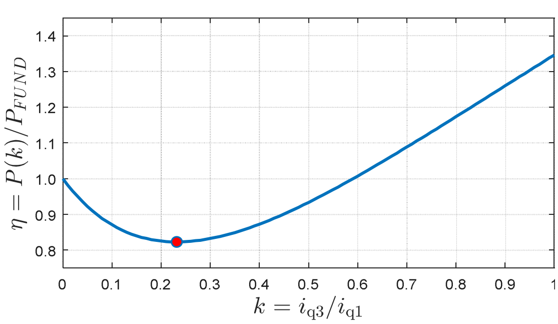

Fig. 4. Average loss in the asymmetrical 12-phase machine case.

From the analysis of the angle set it can be verified that the rectangular matrix built with $[C_1]$, $[C_3]$, and $[C_0]$ has a rank 5, meaning that it is possible to independently control both $\mathbf{i}_1$ and $\mathbf{i}_3$ and, therefore, exploit the third-harmonic contribution for the torque development. However, the rows $[C_9]$ are linearly dependent on the rows $[C_1]$, $[C_3]$, and $[C_0]$, meaning that the control of $\mathbf{i}_1$ and $\mathbf{i}_3$ makes it impossible to simultaneously control also $\mathbf{i}_9$. As a result, for the considered case study, the matrix [C] has been built by choosing the rows related to the space vectors $\mathbf{i}_1$, $\mathbf{i}_3$, $\mathbf{i}_5$, $\mathbf{i}_7$, and $\mathbf{i}_{11}$, while the second zero sequence component i_0^- has been arbitrarily defined through the row $[C_0^-] = \sqrt{1/6} \cdot [1\ 1\ 1\ {-1}\ {-1}\ {-1}\ 1\ 1\ 1\ {-1}\ {-1}\ {-1}]$. The analytical evaluation of the matrix $[H]$ results in $H_1 = 1$; $H_3 = 4$; $H_5 = 1$; $H_7 = 1$; $H_{11} = 1$; $H_{0^-} = 2 - \sqrt{2}$; and $H_0 = 2 \cdot (2 + \sqrt{2})$.

Fig. 4 shows the normalized power losses obtained by exploiting i_{q1} and i_{q3} with a varying injection ratio. Again, in accordance with (21) and (24), the minimum value is obtained for $k \cong 0.23$ and it leads to the power ratio $\eta \cong 0.82$, corresponding to power loss reduction of about 18%.

The optimal phase current waveforms and their spectra are depicted in Fig. 5, normalized by $I_{\mathrm{FUND}} = (2/12) \cdot T_{em}^*/\lambda_{M1}$. As in the previous case, only the first and third-harmonics are present in the current spectra. Again, the waveforms of each three-phase $\{a, b, c\}$ set are identical and just mutually shifted by 120°, while the different sets behave differently from each other. However, in contrast to the nine-phase machine, in this case the magnitude of the third harmonic component is equal in all the windings, meaning that the overall power losses are equally distributed among all the phases. In particular, the third harmonic current components have the same phase in each set, and the pairs $\{a_1, b_1, c_1\}$-$\{a_3, b_3, c_3\}$ and $\{a_2, b_2, c_2\}$-$\{a_4, b_4, c_4\}$ show an opposite sign. This is a direct consequence of the arbitrary definition of i_0^-. Indeed, the control condition $i_0^- = 0$ (resulting from the choice of $[C_0^-]$ and from the optimization with a constant $[i_{dq}]$ set), together with the winding constraint $i_0 = 0$, corresponds to

$$i_{a_1} + i_{b_1} + i_{c_1} + i_{a_3} + i_{b_3} + i_{c_3} = 0;$$
$$i_{a_2} + i_{b_2} + i_{c_2} + i_{a_4} + i_{b_4} + i_{c_4} = 0 \tag{26}$$

which reflect the constraints imposed to a system built from two isolated asymmetrical six-phase winding sets shifted by 15°.

In this context, the capability of enhancing the torque generation by controlling $\mathbf{i}_3$ might lead to an apparent contradiction since, as previously stated, it is impossible to exploit the third harmonic injection in an asymmetrical six phase machine. However, for the considered twelve-phase machine, $\mathbf{i}_3$ results from the superposition of the third harmonic space vectors $\mathbf{i}_3^{[A]}$ and $\mathbf{i}_3^{[B]}$ driven by the currents of the two six-phase windings sets. By denoting as I_3 the magnitude of the optimal third harmonic component in the phase domain it can be verified that these space vectors can be expressed as $\mathbf{i}_3^{[A]} = 3\sqrt{2}\, M_3 I_3 \cos(3\theta) \mathrm{e}^{-\mathrm{j}\pi/4}$ and $\mathbf{i}_3^{[B]} = 3\sqrt{2}\, M_3 I_3 \cos(3\theta - 3\pi/4)$(with $M_3 = \sqrt{(2/3)}$): they generate two pulsating fields in the machine's air-gap and the resulting twelve-phase space vector is equal to $\mathbf{i}_3 = \mathbf{i}_3^{[A]} + \mathbf{i}_3^{[B]} = 3 M_3 I_3 \mathrm{e}^{\mathrm{j}(3\theta - \pi/2)}$, which yields a rotating field at a 3ω angular frequency and justifies the unexpected property.

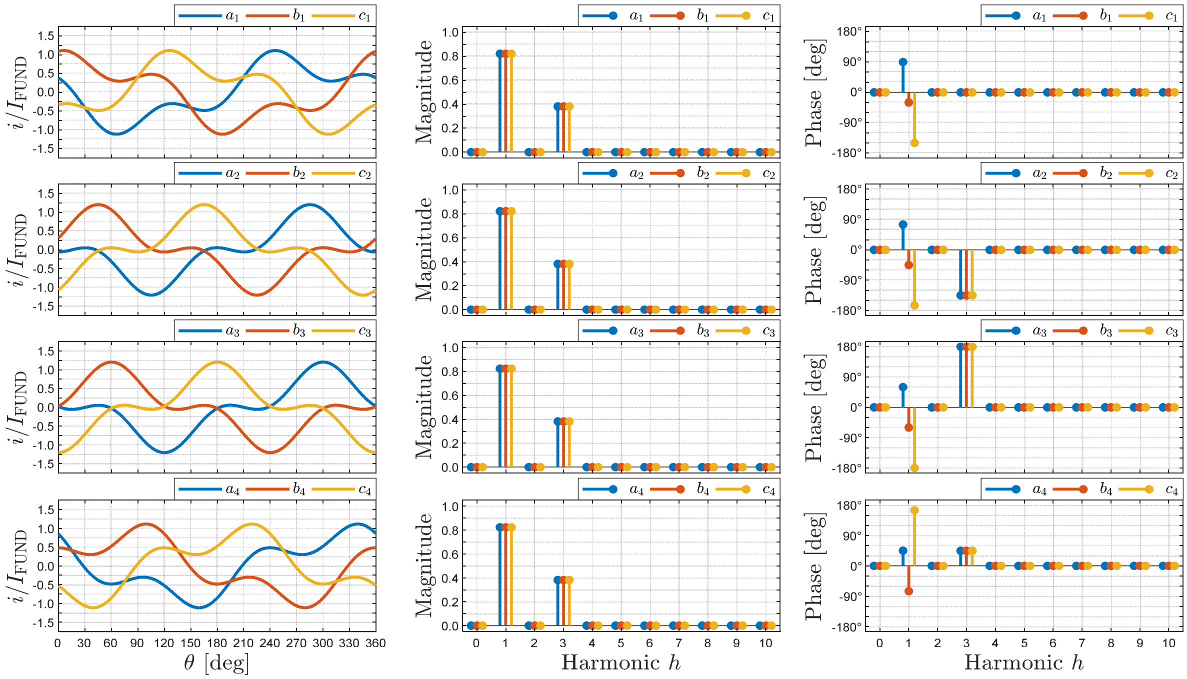

Fig. 5. Optimal phase current waveforms and harmonic spectra for an asymmetrical 12-phase machine.

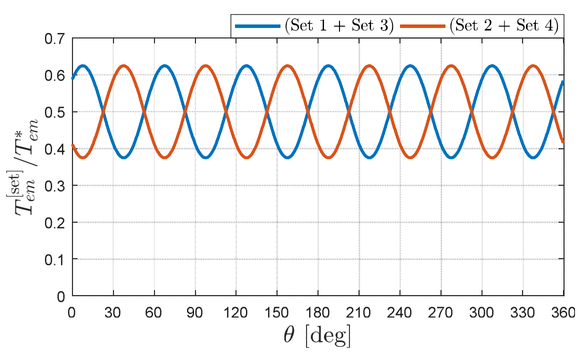

Fig. 6. Torques produced by the two six-phase windings sets.

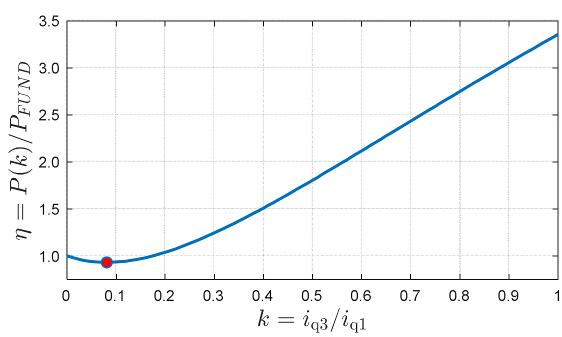

Fig. 7. Average loss in the asymmetrical 15-phase machine case.

From a different perspective, it is possible to observe in Fig. 6 the torques (calculated analytically) generated by applying the optimal reference currents to the two six-phase winding sets—the two contributions present an average value of $T_{em}^*/2$ and a superimposed oscillation varying with 6θ. A single six-phase contribution would not be able to guarantee a constant output torque, whereas their sum cancels out the sinusoidal oscillation.

D. Fifteen-Phase Asymmetrical Machine

The machine windings are here grouped into five symmetrical three-phase sets $\{a_p, b_p, c_p\}$ (with $p = 1, \ldots, 5$), whose magnetic axes are mutually shifted by 12°. Once again, the machine parameters are assumed to be the ones of Table I.

From the analysis of the corresponding Clarke's matrix $[C]$, it can be verified that all the odd-order space vectors up to $\mathbf{i}_{13}$ can be independently controlled at the same time. The evaluation of the matrix $[H]$ results in $H_1 = 1$; $H_3 = 7 + 2\sqrt{5}$; $H_5 = 1$; $H_7 = 1$; $H_9 = 7 - 2\sqrt{5}$; $H_{11} = 1$; $H_{13} = 1$; and $H_0 = 25$.

Fig. 7 shows the normalized power losses obtained with the third harmonic injection. The minimum value is obtained for $k \cong 0.08$ and it leads to the power ratio $\eta \cong 0.93$, corresponding to power loss reduction of about 7%; the optimal phase current waveforms and their spectra are depicted in Fig. 8, normalized by $I_{\mathrm{FUND}} = (2/15) \cdot T_{em}^*/\lambda_{M1}$.

As in the previous cases, the waveforms of each three-phase $\{a, b, c\}$ set are identical and just mutually shifted by 120°, while the different sets behave differently. Similarly to the nine-phase example, in order for the condition $i_0 = 0$ to be satisfied, the third harmonic component is not equally shared by all the windings. Once again, this leads to an unequal distribution of the power losses among the different winding sets. It can be verified from the harmonic spectra that the first and fifth sets have the same magnitude for all the harmonics and, therefore, the same rms. Each of them is responsible for about 19.76% of the total losses.

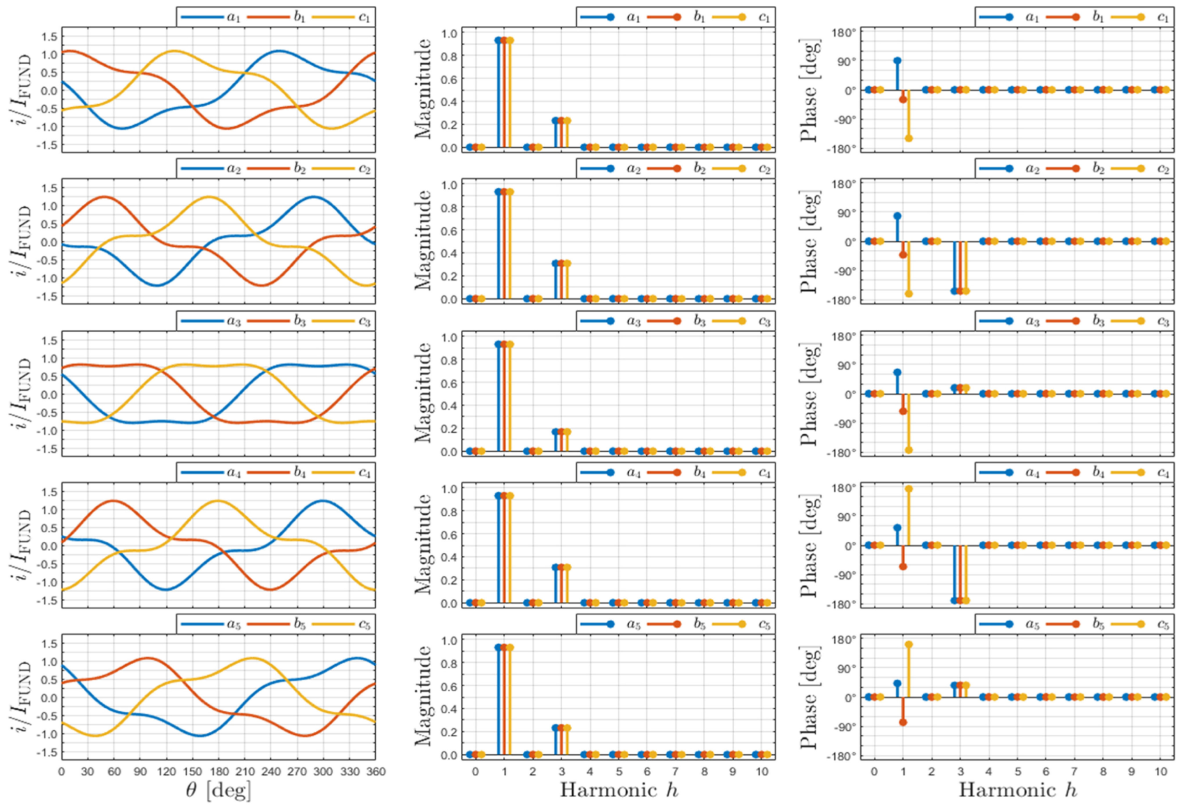

Fig. 8. Optimal phase current waveforms and harmonic spectra for the asymmetrical 15-phase machine.

Analogously, the second and fourth sets behave in the same way and are responsible for about the 20.64% of the total losses, each. Finally, the remaining 19.20% of the losses are dissipated by the third three-phase set.

E. Five-Phase Asymmetrical Machine

This case study focuses on an asymmetrical five-phase machine, obtained from an original symmetrical seven-phase machine after a post-fault reconfiguration in which two adjacent phase windings (i.e., mutually shifted by 360°/7) have been physically disconnected. The resulting phases (further on referred to as $\{a, b, c, d, e\}$) can be identified through the magnetic axis angles set $[\alpha] = [0\ 1\ 2\ 3\ 4]\cdot(360°/7)$. It is assumed that only the first and the third spatial harmonics are present in the permanent magnet flux ($h < n$ assumption) for simplicity and that the PM's induced fluxes have the same values as in the previous examples (i.e., $\lambda_{M1} = 385$ mWb, $\varphi_1 = 0°$, $\lambda_{M3} = 119$ mWb, $\varphi_3 \cong 180°$).

The Clarke's transformation matrix, built using $[C_1]$, $[C_3]$, and $[C_0]$, is full-ranked and the evaluation of the weighting matrix $[H]$ results in $H_1 \cong 1.570$, $H_3 \cong 1.315$, and $H_0 \cong 1.633$.

Fig. 9 shows the normalized power losses for a varying injection ratio—in this case, the optimal injection ratio is obtained for $k \cong 1.11$ (i.e., $i_{\mathrm{q}3} > i_{\mathrm{q}1}$), resulting in $\eta \cong 0.49$, and thus, leading to a power loss reduction of more than 50%.

Fig. 10 shows the phase current waveforms and their corresponding harmonic spectra, first when the machine is controlled by only exploiting $i_{\mathrm{q}1}$ (top plots) and then when $i_{\mathrm{q}3}$

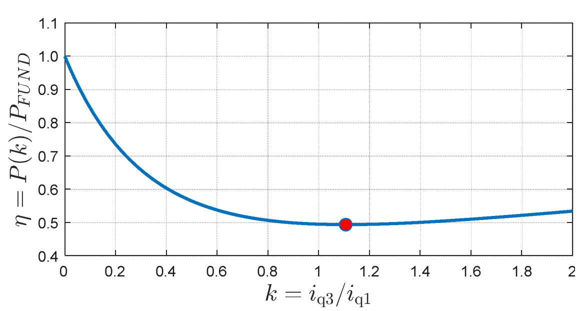

Fig. 9. Average loss in the asymmetrical five-phase machine case.

is simultaneously controlled with the optimal injection ratio (bottom graphs). All the currents have been normalized by $I_{\mathrm{FUND}} = (2/7)\cdot T^*_{em}/\lambda_{M1}$, which is the peak value of the phase currents obtained when the original (i.e., symmetrical seven-phase) machine is driven by only the fundamental current components.

As can be seen, in contrast to the previous examples, in this case the phase current waveforms are mutually different even when only the fundamental component is controlled. In both operating conditions the magnitudes of the harmonic components of phase a are equal to the ones of phase e, while the magnitudes of the harmonic components of phase b are equal to the ones of phase d. They differ from those in phase c.

When only the first harmonic component is exploited, phases a and e are responsible for 18.61% of the overall losses each, phase b and d are responsible for 11.97% each, while phase

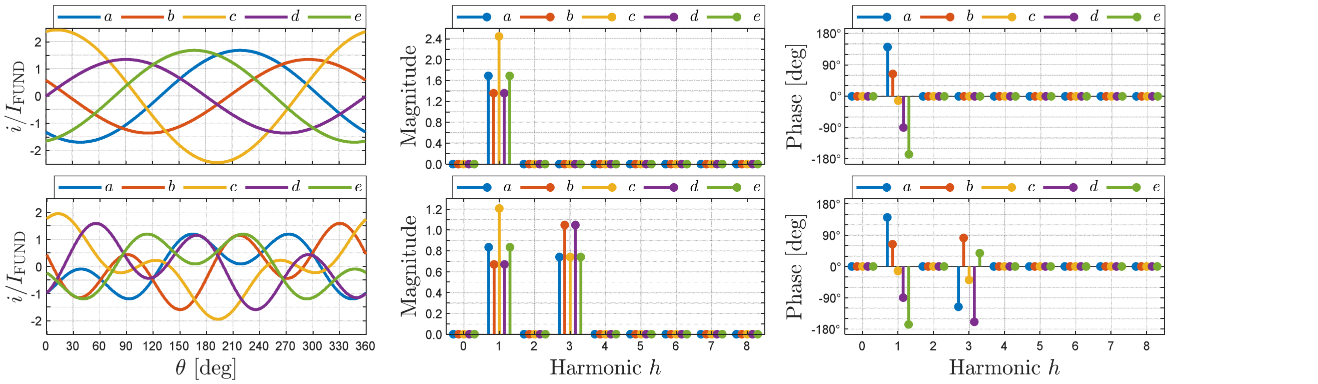

Fig. 10. Phase current waveforms and harmonic spectra for the asymmetrical five-phase machine (Top: Fundamental only; Bottom: Optimal third-harmonic injection).

c is responsible for the remaining 38.85%. By injecting the optimal third harmonic current component, the power losses in phase a and e reduce and are 16.42% of the total, the losses in phase b and d increase and become 20.38% of the total, while the power dissipated in phase c is lowered to 26.41% of the overall losses. It can be concluded that, for the considered example, the harmonic injection is able to not only drastically improve the machine's overall energetic performances, but it is also responsible for a better redistribution of the power losses, if compared to the solely fundamental excitation. Moreover, the peak current of phase c (which, in both scenarios, is the highest one) is reduced by around 20%, thanks to the reduction of the fundamental component allowed by the injection of the additional third harmonics.

V. Numerical and Experimental Results

The proposed approach has been numerically and experimentally validated with respect to the asymmetrical nine-phase machine described in [22] and [23]. From the analysis of the electrical equations in the synchronous domain [obtained through (18)] it can be verified that the first, fifth, and seventh space vector subspaces are decoupled, resulting in [22]

$$\begin{cases} u_{dh} = v_{dh} = Ri_{dh} + L_h \frac{\mathrm{d}i_{dh}}{\mathrm{d}t} - h\omega L_h i_{qh} \\ u_{qh} = v_{qh} = Ri_{qh} + L_h \frac{\mathrm{d}i_{qh}}{\mathrm{d}t} + h\omega L_h i_{dh} + e_{qh} \end{cases} \tag{27}$$

with h = 1,5,7 and $e_{\mathrm{qh}} = \sqrt{9/2}h\omega\lambda_{Mh}$. The third space vector subspace is instead coupled with v_{ON} by $[g](\theta)$ [22]

$$\begin{cases} u_{d3} + 2\sqrt{2}\cos(3\theta + \varphi_3 - \pi/3) \cdot v_{\mathrm{ON}} = v_{d3} \\ = Ri_{d3} + L_3 \frac{\mathrm{d}i_{d3}}{\mathrm{d}t} - 3\omega L_3 i_{q3} \\ u_{q3} + 2\sqrt{2}\cos(3\theta + \varphi_3 + \pi/6) \cdot v_{\mathrm{ON}} = v_{q3} \\ = Ri_{q3} + L_3 \frac{\mathrm{d}i_{q3}}{\mathrm{d}t} + 3\omega L_3 i_{d3} + e_{q3} \end{cases} \tag{28}$$

with e_{q3}= $9/\sqrt{2}\omega\lambda_{M3}$. It should also be noted that, given the asymmetrical winding configuration, v_{ON} is itself dependent on the currents (i_{d3}, i_{q3}). Indeed, by imposing the conditions i_0 = 0 and $\mathrm{d}i_0/\mathrm{d}t$ = 0 in the zero-sequence equation of the model

TABLE II
Nine-Phase Machine Electrical Parameters

R = 31.3 Ω	L_1 = 147 mH	L_5 = 88 mH
L_l = 84 mH	L_3 = 92 mH	L_7 = 87 mH

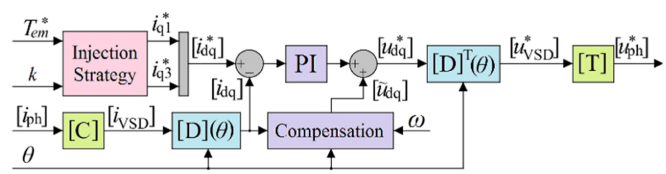

Fig. 11. Control scheme.

(18), the following functional relationship is obtained:

$$\begin{cases} v_{ON} = \frac{L_{m3}}{9}\left[\left(2\sqrt{2}\sin(3\theta+\varphi_3+\pi/6)\right)\left(\frac{\mathrm{d}\,i_{\mathrm{d3}}}{\mathrm{d}t} - 3\omega i_{\mathrm{q3}}\right) + \ldots\right. \\ \left.\ldots + \left(2\sqrt{2}\cos(3\theta+\varphi_3+\pi/6)\right)\left(\frac{\mathrm{d}\,i_{\mathrm{q3}}}{\mathrm{d}t} + 3\omega i_{\mathrm{d3}}\right)\right] + \frac{e_0 - u_0}{3} \end{cases} \tag{29}$$

with $L_{m3} = L_3 – L_l$ and $e_0 = -6\omega\lambda_{M3}\sin(3\theta + \varphi_3 - \pi/3)$. The additional coupling terms arising among the (i_{d3}, i_{q3}) components, which can be identified by substituting (29) in (28), need to be properly compensated in the current control. It is important to highlight that the supplying inverter's common mode voltage influences both u_0 and (u_{d3}, u_{q3}) at the same time, such that their simultaneous changes cancel out and do not affect the (i_{d3}, i_{q3}) current dynamics. Therefore, the compensation of e_0 can be achieved either by acting on u_0 or by acting on both u_{d3} and u_{q3}.

The machine under analysis has one pole pair, its flux parameters correspond to the ones reported in Table I, while its electrical parameters are reported in Table II.

A. Simulation Results

The numerical results have been obtained in the MATLAB/Simulink environment. The implemented control algorithm is schematically represented in Fig. 11.

The "injection strategy" block finds the references i^*_{q1} and i^*_{q3} able to develop the desired electromagnetic torque T^*_{em} for a given injection ratio $k = i^*_{q3}/i^*_{q1}$; obviously, when $k = k_{\mathrm{opt}}$

the block implements the developed optimal injection strategy and selects the references according to (22). All the other components of the reference set $[i^*_{dq}]$ are zero.

Since the reference current set $[i^*_{dq}]$ is constant, a proportional–integral (PI) controller has been used to drive all the components of the synchronous current set $[i_{dq}]$ (with the only exception of $i_0 = 0$ which, obviously, cannot be controlled due to the hardware constraint). While the compensation terms in the first, fifth, and seventh space vectors' subspaces are obtained by the standard FOC approach, the third space vector subspace needs an additional compensation term to neutralize the effects of v_{ON}. Based on the model equations (27)–(29), the "Compensation" block represented in Fig. 11 computes the voltage set $[\tilde{u}_{dq}]$ through the relations

$$\left.\begin{aligned}\tilde{u}_{dh} &= -h\omega L_h i_{qh}\\ \tilde{u}_{qh} &= +h\omega L_h i_{dh} + e_{qh}\end{aligned}\right\} \quad \text{with} \quad h = 1, 5, 7$$

$$\tilde{u}_{d3} = -3\omega L_3 i_{q3} - 2\sqrt{2}\cos(3\theta + \varphi_3 - \pi/3) \cdot \tilde{v}_{\mathrm{ON}}$$

$$\tilde{u}_{q3} = +3\omega L_3 i_{d3} - 2\sqrt{2}\cos(3\theta + \varphi_3 + \pi/6) \cdot \tilde{v}_{\mathrm{ON}} + e_{q3}$$

$$\tilde{u}_0 = e_0 = -6\omega\lambda_{M3}\sin(3\theta + \varphi_3 - \pi/3) \tag{30}$$

with $\tilde{v}_{\mathrm{ON}} = (2\sqrt{2}\omega L_{m3}/3)[i_{d3}\cos(3\theta + \varphi_3 + \pi/6) - i_{q3}\sin(3\theta + \varphi_3 + \pi/6)]$.

The resulting vector is added to the output of the current PI controllers and it represents the synchronous voltage set $[u^*_{dq}]$, which is finally transformed into the corresponding inverter's reference voltage set $[u^*_{ph}]$ by applying the inverse transformations (7) and (11).

The control algorithm has been implemented in discrete time with a 10-kHz sampling frequency. The supplying inverter has been simulated through an average model to filter out the high frequency harmonics introduced by the pulsewidth modulation technique.

Fig. 12 shows the simulation results obtained by implementing the proposed injection strategy in a feedback controller, which keeps the machine speed at 500 r/min with a constant load torque of 2 N·m. The injection ratio $k = i_{q3}/i_{q1}$ has been linearly changed from 0 to 1 in a 20 s time span and all the other components of $[i_{dq}]$ are kept to zero.

Consistently with the theoretical results, the optimal condition is obtained for $k \cong 0.19$, where the power losses are effectively reduced from an initial value of about 188 W to the minimum value of about 160 W.

B. Experimental Results

The experimental validation of the theoretical results has been performed using the nine-phase PMSM described in [23], whose windings have been properly rearranged to an asymmetrical configuration. The shaft of the PMSM has been coupled to a dc machine (used for loading) by a Datum Electronics M425 torque meter (see Fig. 13(a)). The machine has been supplied using two custom-made multiphase inverters, based on Infineon FS50R12KE3 IGBT modules (see Fig. 13(b)). They have a common dc link, whose voltage is equal to 450 V and is supplied by a Sorensen SGI600/25 single quadrant dc-voltage source. The switching frequency of the inverter has been set to 5 kHz. The control algorithm has been implemented with a dSPACE ds1006 platform working at 10 kHz. An ADC board (ds2004) has been used to acquire the phase currents measured by the inverter's internal LEM sensors, while an incremental encoder board (ds3002) has provided the speed/position from the encoder. Additional measurements have been recorded using a Tektronix DPO/MSO 2014 oscilloscope, equipped with TCP0030A current probes.

The measured value of one induced back-EMF waveform (phase a_1) and the corresponding harmonic spectrum are depicted in Fig. 14. The magnitude spectrum is normalized by the fundamental harmonic, while the phase spectrum is shifted in order to obtain a phase of 90° for the fundamental component

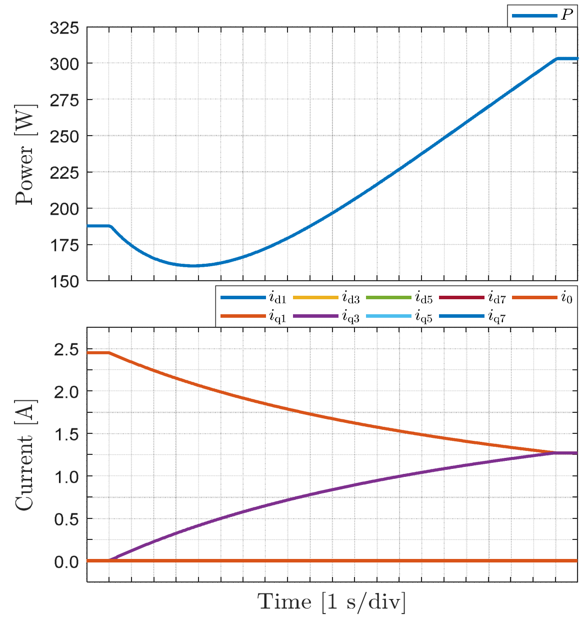

Fig. 12. Simulation results for the asymmetrical nine-phase case.

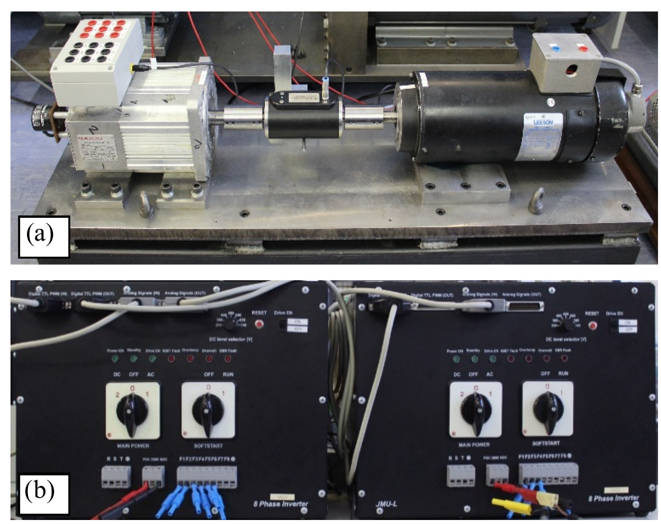

Fig. 13. Experimental test bench for the asymmetrical nine-phase drive. (a) Nine-phase PMSM and dc load. (b) Multiphase inverters.

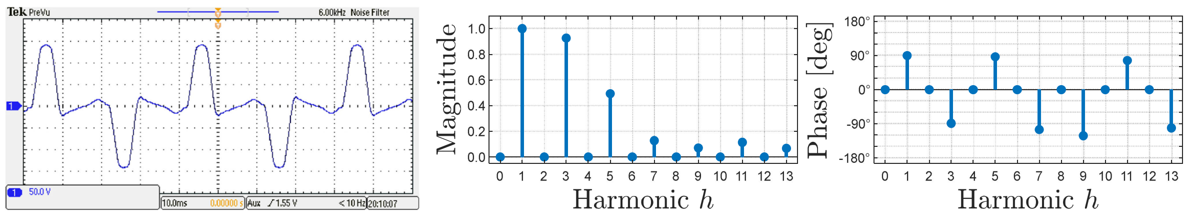

Fig. 14. PM induced back-EMF waveform (left, obtained at around 1500 r/min) and harmonic spectrum (right, normalized by the fundamental).

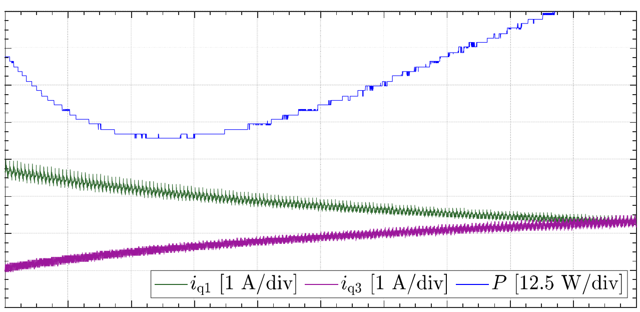

Fig. 15. Average losses (P), and quadrature currents (i_{q1}, i_{q3}) for a linearly varying injection ratio ($k = i_{q3}/i_{q1}$) in a 20 s time window (2 s/div).

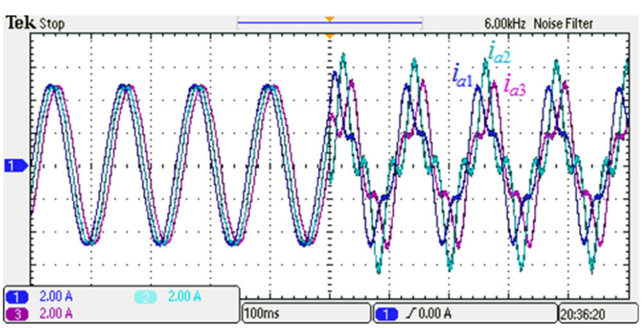

Fig. 16. Phase currents (multiplied by 4) without/with the optimal third-harmonic injection.

(i.e., in this way the phase φ_1 of the fundamental component of the corresponding flux $\lambda_{a_1} = \int_0^t e_{a_1}(\tau)\mathrm{d}\tau$ is set to zero).

The experiment follows the scenario described in the previous subsection—the i_{q1} and i_{q3} currents have been exploited for the torque development and the test has been performed by linearly varying the ratio $k = i_{q3}/i_{q1}$ in the interval [0; 1] during a time window of 20 s. The machine runs at a constant speed of 500 r/min with a load torque of about 2 N·m.

Fig. 15 shows the average stator power losses P and the quadrature currents i_{q1} and i_{q3} (obtained by processing measured currents) during the testing interval. The resulting waveforms are very similar to the corresponding simulation results depicted in Fig. 12. The minimum dissipation is reached around 4.5 s; it corresponds to $k \cong 0.22$, which is reasonably close to the theoretical optimal ratio $k_{\mathrm{opt}} \cong 0.19$ obtained from (21).

In Fig. 16, the $\{a_1, a_2, a_3\}$ current waveforms without and with the optimal third-harmonic injection are shown. They have been obtained by step-changing the injection ratio k from zero to the theoretical optimal value $k \cong 0.19$. As is evident, after an initial short transient, there is a good agreement with the corresponding theoretical current waveforms depicted in Fig. 3.

VI. Conclusion

This article presented a modeling approach and an optimal strategy to exploit a third-harmonic current injection for the torque enhancement in multiphase isotropic PMSMs with non-sinusoidal back-EMFs.

The modeling approach was presented for a generic (i.e., asymmetrical, with an arbitrary angular shift) winding configuration and was based on the VSD and rotational transformation. The torque developed by the machine could be expressed as a linear combination of the quadrature components of the currents space vectors linked to each harmonic contribution.

The choice of a proper Clarke's transformation matrix was crucial to select the desired harmonics, which could be effectively controlled. In a general case (and contrary to the symmetrical winding configurations), the transformation matrices are not unitary. This affects the power loss expression, which weights differently each current harmonic component. Moreover, when the machine's electrical equations are expressed using the transformed variables, the asymmetrical machine configuration usually leads to coupling among the different space vectors, which should be properly compensated in the current control.

Once the transformed set had been chosen, the proposed strategy was based on the choice of a constant current set in the multiple synchronous domain. This choice greatly simplified the power loss expression, it allowed to directly relate each current space vector to a given steady-state harmonic injected into the phase currents, and it made it possible to design the feedback controller via PI regulators and compensating actions. The strategy chose a constant i_{q1} (responsible for the fundamental currents) and a constant i_{q3} (responsible for the third-harmonic injection). Their ratio was computed in a way which minimized the average winding losses for a given torque. This problem had an analytical solution which only depended on the magnitude of the PM induced fluxes and on the stator windings' disposition.

The strategy was particularized for some specific asymmetrical configurations (including those where symmetrical winding was preferred, such as 9- and 15-phase) in order to highlight its properties. An experimental validation was also performed using an asymmetrical nine-phase machine. Both the simulation and the experimental results were in a good agreement with the theoretical analysis.

REFERENCES

[1] E. Levi, "Multiphase electric machines for variable-speed applications," *IEEE Trans. Ind. Electron.*, vol. 55, no. 5, pp. 1893–1909, May 2008.

[2] E. Levi, F. Barrero, and M. J. Duran, "Multiphase machines and drives–revisited," *IEEE Trans. Ind. Electron.*, vol. 63, no. 1, pp. 429–432, Jan. 2016.

[3] E. Levi, R. Bojoi, F. Profumo, H. A. Toliyat and S. Williamson, "Multiphase induction motor drives–A technology status review," *IET Elect. Power Appl.*, vol. 1, no. 4, pp. 489–516, Jul. 2007.

[4] M. Farshadnia, M. A. Masood Cheema, A. Pouramin, R. Dutta, and J. E. Fletcher, "Design of optimal winding configurations for symmetrical multiphase concentrated-wound surface-mount PMSMs to achieve maximum torque density under current harmonic injection," *IEEE Trans. Ind. Electron.*, vol. 65, no. 2, pp. 1751–1761, Feb. 2018.

[5] K. Wang, Z. Q. Zhu, and G. Ombach, "Torque enhancement of surface-mounted permanent magnet machine using third-order harmonic," *IEEE Trans. Magn.*, vol. 50, no. 3, pp. 104–113, Mar. 2014.

[6] K. Wang, Z. Y. Gu, Z. Q. Zhu, and Z. Z. Wu, "Optimum injected harmonics into magnet shape in multiphase surface-mounted PM machine for maximum output torque," *IEEE Trans. Ind. Electron.*, vol. 64, no. 6, pp. 4434–4443, Jun. 2017.

[7] J. Wang, L. Zhou, and R. Qu, "Harmonic current effect on torque density of a multiphase permanent magnet machine," in *Proc. Int. Conf. Elect. Mach. Syst.*, 2011, pp. 1–6.

[8] Z. Q. Zhu, K. Wang, and G. Ombach, "Optimal magnet shaping with third order harmonic for maximum torque in SPM machines," in *Proc. 6th IET Conf. Power Electron., Mach. Drives*, 2012, pp. 1–6.

[9] L. Parsa and H. A. Toliyat, "Five-phase permanent magnet motor drives," *IEEE Trans. Ind Appl.*, vol. 41, no. 1, pp. 30–37, Jan./Feb. 2005.

[10] L. Parsa and H. A. Toliyat, "Five-phase permanent magnet motor drives for ship propulsion applications," in *Proc. Elect. Ship Tech. Symp.*, 2005, pp. 371–378.

[11] P. J. McCleer, J. M. Bailey, J. S. Lawler, and B. Banerjee, "Five phase trapezoidal back EMF PM synchronous machines and drives," in *Proc. Eur. Power Electron. Appl. Conf.*, 1991, pp. 128–133.

[12] K. Wang, Z. Y. Gu, C. Liu, and Z. Q. Zhu, "Design and analysis of a five-phase SPM machine considering third harmonic current injection," *IEEE Trans. Energy Convers.*, vol. 33, no. 3, pp. 1108–1117, Sep. 2018.

[13] L. Parsa, N. Kim, and H. A. Toliyat, "Field weakening operation of high torque density five-phase permanent magnet motor drives," in *Proc. IEEE Int. Elect. Mach. Drives Conf.*, 2005, pp. 1507–1512.

[14] B. Aslan and E. Semail, "New 5-phase concentrated winding machine with bi-harmonic rotor for automotive application," in *Proc. Int. Conf. Elect. Mach.*, 2014, pp. 2114–2119.

[15] Y. Sui, P. Zheng, Y. Fan, and J. Zhao, "Research on the vector control strategy of five-phase PMSM based on third-harmonic current injection," in *Proc. IEEE Int. Elect. Mach. Drives Conf.*, 2017, pp. 1–8.

[16] Z. Y. Gu, K. Wang, Z. Q. Zhu, Z. Z. Wu, C. Liu, and R. W. Cao, "Torque improvement in five-phase unequal tooth SPM machine by injecting third harmonic current," *IEEE Trans. Veh. Technol.*, vol. 67, no. 1, pp. 206–215, Jan. 2018.

[17] J. Gong, H. Zahr, E. Semail, M. Trabelsi, B. Aslan, and F. Scuiller, "Design considerations of five-phase machine with double p/3p polarity," *IEEE Trans. Energy Convers.*, vol. 34, no. 1, pp. 12–24, Mar. 2019.

[18] Y. Hu, Z. Q. Zhu, and M. Odavic, "Torque capability enhancement of dual three-phase PMSM drive with fifth and seventh current harmonics injection," in *Proc. 22nd Int. Conf. Elect. Mach.*, 2016, pp. 599–605.

[19] R. O. C. Lyra and T. A. Lipo, "Torque density improvement in a six-phase induction motor with third harmonic current injection," *IEEE Trans. Ind Appl.*, vol. 38, no. 5, pp. 1351–1360, Sep./Oct. 2002.

[20] B. Stumberger, G. Stumberger, A. Hamler, M. Trlep, M. Jesenik, and V. Gorican, "Increasing of output power capability in a six-phase flux-weakened permanent magnet synchronous motor with a third harmonic current injection," *IEEE Trans. Magn.*, vol. 39, no. 5, pp. 3343–3345, Sep. 2003.

[21] K. Wang, J. Y. Zhang, Z. Y. Gu, H. Y. Sun, and Z. Q. Zhu, "Torque improvement of dual three-phase permanent magnet machine using zero sequence components," *IEEE Trans. Magn.*, vol. 53, no. 11, pp. 1–4, Nov. 2017.

[22] A. Cervone, M. Slunjski, E. Levi, and G. Brando, "Optimal third-harmonic current injection for an asymmetrical nine-phase PMSM with non-sinusoidal back-EMF," in *Proc. 45th Ann u . Conf. IEEE Ind. Electron. Soc.*, 2019, pp. 6223–6228.

[23] M. Slunjski, M. Jones, and E. Levi, "Analysis of a symmetrical nine-phase machine with highly non-sinusoidal back-EMF force," in *Proc. 44th Ann. Conf. IEEE Ind. Electron. Soc.*, 2018, pp. 6229–6234.

Andrea Cervone (Student Member, IEEE) received the B.Sc. and M.Sc. degrees in electrical engineering in 2014 and 2017, respectively, from the University of Naples Federico II, Naples, Italy, where he is currently working toward the Ph.D. degree in electrical engineering.

His research interests include multilevel converters and electrical drives.

Marko Slunjski (Student Member, IEEE) received the B.Sc. and M.Sc. degrees in electrical engineering from the Faculty of Electrical Engineering and Computing, University of Zagreb, Zagreb, Croatia, in 2015 and 2017, respectively. Since July 2017, he has been with Liverpool John Moores University, Liverpool, U.K., where he is working toward the Ph.D. degree in electrical engineering.

His research interests include power electronics and advanced variable speed multiphase drive systems.

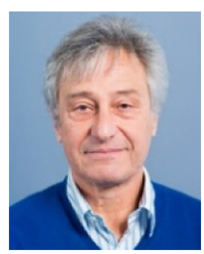

Emil Levi (Fellow, IEEE) received the M.Sc. and the Ph.D. degrees in electrical engineering from the University of Belgrade, Belgrade, Serbia, in 1986 and 1990, respectively.

He joined Liverpool John Moores University, Liverpool, U.K. in May 1992 and is a Professor of Electric Machines and Drives, since September 2000.

Dr. Levi served as a Co-Editor-in-Chief of the IEEE TRANSACTIONS ON INDUSTRIAL ELECTRONICS during 2009–2013. Currently, he is the Editor-in-Chief of the IEEE TRANSACTIONS ON INDUSTRIAL ELECTRONICS, Editor-in-Chief of the *IET Electric Power Applications*, and an Editor of the IEEE TRANSACTIONS ON ENERGY CONVERSION. He was the recipient of the Cyril Veinott award of the IEEE Power and Energy Society for 2009 and the Best Paper award of the IEEE TRANSACTIONS ON INDUSTRIAL ELECTRONICS for 2008. In 2014, he received the "Outstanding Achievement Award" from the European Power Electronics (EPE) Association and in 2018 the "Professor Istvan Nagy Award" from the Power Electronics and Motion Control (PEMC) Council.

Gianluca Brando received the M.S. (cum laude) and Ph.D. degrees in electrical engineering from the University of Naples Federico II, Naples, Italy, in 2000 and 2004.

From 2000 to 2012, he was a Postdoctoral Research Fellow with the Department of Electrical Engineering, University of Naples Federico II. Since 2012, he is an Assistant Professor of Electrical Machines and Drives with the Department of Electrical Engineering and Information Technology, University of Naples Federico II. He has authored several scientific papers published in international journals and conference proceedings. His research interests include control strategies for power converters and electrical drives.